RSC Advances

PAPER

View Article Online
View Journal | View Issue

Cite this: *RSC Adv.*, 2023, **13**, 28852

Synthesis of an eco-inspired anticorrosive composite for mild steel applications

Anoja Kawsihan,[ab] D. M. S. N. Dissanayake,[b] N. P. W. Rathuwadu,[c] H. C. S. Perera,[g] K. E. D. Y. T. Dayananda,[d] K. R. Koswattage,[ef] Rajesh Mahadeva,[g] Arnab Ganguly,[g] G. Das *[g] and M. M. M. G. P. G. Mantilaka *[df]

We synthesised a polyaniline/mica (Mica–PANI) nanocomposite using naturally occurring muscovite mica by a top-down approach. The developed coating materials were characterised using a different technique to investigate their chemical and structural properties using Fourier transform infrared spectroscopy (FTIR), X-ray diffraction (XRD), scanning electron microscopy (SEM), X-ray photoelectron spectroscopy (XPS), and thermogravimetric analysis (TGA). Furthermore, the electrochemical properties of the coating materials were investigated by linear sweep voltammetry (LSV). SEM images elucidate the composite's average particle diameter of the prepared nano-mica, approximately 80 nm. The existence of relevant functional groups and bonding in the prepared Mica–PANI composite material was confirmed by means of XPS and FTIR techniques. Moreover, the synthesised composite with 5% w/w shows high anticorrosion protection, *i.e.* 84 μm per year, compared to competing materials, including commercial paint and individual raw materials (0.35 mm per year). The anti-corrosive effect occurs mainly due to two opposing effects: the formation of an $Fe(OH)_3$ passive layer on the steel surface by oxidation of surface iron atoms by the PANI and the barrier effect of mica NPs through inhibition of corrosive agents. Therefore, the eco-inspired composite could be an ideal cost-effective coating material to prevent the corrosion of mild steel surfaces.

Received 30th April 2023
Accepted 8th September 2023

DOI: 10.1039/d3ra02857g

rsc.li/rsc-advances

Introduction

Degrading metals through the corrosion process has become a significant challenge to ensure the durability of metal products and surfaces. Accordingly, corrosion protection has been a vital topic among scientists, engineers, manufacturers, and product consumers in recent years and for many decades.[1] The currently available techniques to protect metal structures from corrosion include applying special protective organic or metallic coatings, galvanising, corrosion inhibitors, *etc.*[2–4] Nonetheless, the development of anticorrosive coatings using organic and inorganic materials as composites has attained great interest in the field of research and industries due to their cost effectiveness, the availability of raw materials, effectiveness, superior performance in corrosion protection, and the synergetic properties on the finished product or surface.[5,6] Moreover, the anticorrosive coating, fabricated by grafting corrosion inhibitors directly into nanocarriers and forming nanocomposite coatings, is a promising strategy for protecting metals and metal alloys against a corrosive environment.

PANI is highly utilised due to its fascinating and unique properties such as redox tunability, environmental stability, electrochromic properties, cost-effective/flexible method of production, and forming passivation of oxide layer between metal and coating.[7–9] It is also more attractive as it shows a simple acid–base doping–developing process and three distinct oxidation states with different colours.[10] Alkyd or epoxy resins are generally used to synthesise PANI-based anticorrosive paints, which can protect metals and metal alloys from corrosion.[11] Nevertheless, there are also limitations to using PANI in anticorrosive paint due to its poor adhesion, thermal stability, and low abrasion resistance.[9,12,13]

Muscovite is a phyllosilicate mica mineral with a chemical composition $KAl_2(Al, Si_3O_{10})(F, OH)$ widely found in the natural deposits abundantly.[14] The previous study confirms that muscovite is a more convenient compound that can be utilised for coatings.[15] It also exhibits excellent properties for producing

[a]*Academy of Sri Lanka Institute of Nanotechnology, Nanotechnology and Science Park, Mahenwatte, Pitipana, Homagama, Sri Lanka*
[b]*Sri Lanka Institute of Nanotechnology, Nanotechnology and Science Park, Mahenwatte, Pitipana, Homagama, Sri Lanka*
[c]*Institute for Combinatorial Advanced Research and Education, General Sir John Kotelawala Defence University, Ratmalana, Sri Lanka*
[d]*Institute of Materials Engineering and Technopreneurships (IMETECHNO), Kandy, Sri Lanka. E-mail: mantilaka.publications@gmail.com; mantilaka@gmail.com*
[e]*Department of Engineering Technology, Faculty of Technology, Sabaragamuwa University of Sri Lanka, 70140 Belihuloya, Sri Lanka*
[f]*Centre for Nanodevices Fabrication and Characterization (C. N. F. C.), Faculty of Technology, Sabaragamuwa University of Sri Lanka, 70140 Belihuloya, Sri Lanka*
[g]*Department of Physics, Khalifa University, United Arab Emirates. E-mail: gobind.das@ku.ac.ae*

anticorrosive paint, including structure with chemical stability, low reactivity, compatibility in producing polymer matrices, high electrical and thermal insulation, and protection from U.V. radiation.[16]

This paper describes a novel method to synthesise Mica–PANI nanocomposite using naturally occurring muscovite mica as an anticorrosive coating material on mild steel surfaces. Although, there have been plenty of research based on PANI/montmorillonite nanocomposites, PANI doped with *p*-toluenesulfonate for the anticorrosive performance, this study contributes significantly to the surface protective coating industry as it uses Muscovite mica nanoparticles made with a convenient top-down approach, which is readily available, cost-effective, uncomplicated, nontoxic, insulative, and flexible material. This effort is also significant in value-addition to natural mica deposits in a sustainable manner. Preparing new composite material as an anticorrosive coating for mild steel surfaces is the critical element contributing novelty to the study. Earlier studies have shown that PANI inhibits corrosion through the barrier effect and electrochemical process of forming a passive layer of $Fe(OH)_3$ on the steel surface due to the oxidation of surface iron atoms.[17,18] In this study, the anticorrosion ability of PANI is further increased by the addition of mica nanoparticles due to the barrier effect provided by mica NPs towards corrosive agents.

Experimental

Synthesis

Analytical grades of aniline (~99.5%), stearic acid (octadecanoic acid ~95%), hydrochloric acid (~37%), sodium persulfate (~99.9%), and ethanol (~99.8%) were purchased from Sigma-Aldrich. Commercial grade 2K clear, 2K hardener (Alkyd resin), xylene (thinner), and mild steel were purchased from Sri Lankan open market. Mica samples were collected from Badulla, situated in the lower central hills of Sri Lanka.

Preparation of mica nanoparticles (NPs)

Mica nanoparticles (NPs) were synthesised using a top-down approach. Bulk mica sheets were ground to micron size in the synthesis using a grinder. Then, the ground mica was sieved using a 300 μm mesh strainer to obtain lesser size particles. After that, sieved mica particles were ground using 1 mm silica balls of nano-grinder for 2 h. Finally, the gravity filtration technique separated mica nanoparticles from silica balls.

Preparation of Mica–PANI nanocomposites

To prepare Mica–PANI nanocomposites, 2 g of mica NPs was added to 0.1 M, 25 mL stearic acid in ethanol solution. The solution was heated to 80 °C, and then, 1.5 M, 25 mL of HCl was added and stirred well using a magnetic stirrer until the solution became homogenous. Then, 2 mL of aniline was added to the same solution and stirred further for 30 min. Later, 0.4 M, 25 mL of $Na_2S_2O_8$ was added dropwise into the mixture at the rate of 1 drop per sec. The prepared Mica–PANI composite material was thoroughly washed with 200 mL of distilled water and collected by centrifugation at 6000 rpm. Finally, the collected Mica–PANI composite was dried in a vacuum oven at 40 °C for 8 h.

Chemical characterisation

Fourier transform infrared (FT-IR). FT-IR spectra of the Mica–PANI composite material, mica NPs, and PANI were recorded on Bruker Vertex 80 FT-IR spectrometer with attenuated total reflectance (ATR) in the range of 500–4000 cm^{-1}. The measurements were performed with a resolution of 4 cm^{-1}.

X-ray photoelectron spectroscopy (XPS). The elemental composition of the prepared composite materials and mica NPs was investigated by X-ray photoelectron spectroscopy (XPS) Scienta ESCA 200 spectrometer with Al Kα X-ray source, base pressure $>5 \times 10^{-10}$ mbar and spot size of 300 μm.

Physical characterisation

X-ray diffraction (XRD). The bulk mica prepared mica NPs, PANI, and Mica–PANI composite were characterised using XRD patterns from a Siemens D5000 Powder X-Ray Diffractometer, with the Cu K_α radiation of wavelength $\lambda = 0.1540562$ nm, and the scan rate of 1° min^{-1} to study the crystalline phases. The obtained XRD patterns were examined using X Powder 12 Software with the help of the ICDD PDF2 database. The average crystallite size of the composite was determined by applying the Debye–Scherer equation to the major XRD peaks from mica NPs and Mica–PANI composite.

Thermogravimetric analysis (TGA). Thermal analysis of the prepared Mica–PANI composite material, mica NPs, and PANI was conducted using a TGA STD Q600 from room temperature to 800 °C at the heating rate of 10 °C min^{-1} in N_2 purged condition.

Morphological analysis and elemental analysis. Morphologies and the particle size of the prepared composite materials and mica NPs were observed using scanning electron microscopy (SEM) Hitachi SU6600 with an accelerating voltage of 10 kV and energy dispersive X-ray spectroscopy (EDX) to investigate the elemental composition qualitatively.

Study of anticorrosive property

Mica–PANI composites of 0.34 g (5% w/w), 0.7 g (10% w/w), and 1.25 g (16% w/w) were dispersed separately in a mixture of 2K clear (2.5 g), 2K hardener (0.625 g), and xylene (3.3 g) to prepare the composite mixtures for the coating "a", "b" and "c" respectively to compare the activity of Mica–PANI composite percentages. The ratios of each material of 2K clear, 2K hardener, and xylene were selected according to the procedure mentioned on the label of the products. To compare the activity of individual components of PANI and mica NPs, mixtures for the coatings "d" and "e" were prepared by of 5% w/w PANI and 5% w/w of mica NPs separately with the mixture of 2K clear (2.5 g), 2K hardener (0.625 g) and xylene (3.3 g). The coating "f," which is the "blank" sample, is prepared by mixing 2K clear (2.5 g), 2K hardener (0.625 g), and xylene (3.3 g). The coating "g" with purchased commercial paint was prepared to compare the corrosion inhibition efficiency of the Mica–PANI composite.

Brush coating technique was found to be effective for preparation of each coating among other techniques including spray coating, dip coating and flow coating after series of SEM image investigation. Though, these seven coatings were applied on mild steel immediately using the brush coating technique after polishing the surface with 220 and 400 emery papers and cleaning with acetone and ethanol. The coated area is 1 cm × 1 cm. The thicknesses of the coatings were measured using a digital micrometre screw gauge.

Corrosion studies were carried out on each coated and uncoated (bare) mild steel surface initially (soon after dipping the coating inside the NaCl solution) and after 24 h in the same condition to observe the changes after attaining the equilibrium position inside the solution to confirm the stability of the coatings. The coated and uncoated mild steel was used as the working electrode with a platinum sheet counter electrode and Ag/AgCl reference electrode in 0.1 M NaCl (aq) solution. Linear sweep voltammetry (LSV) studies were carried out for each coating cast on mild steel surfaces. LSV was performed in the potential range from −0.5 V to +0.5 V with respect to the open circuit potential of each sample at the scan rate of 5 mV s^{-1}. The corrosion studies were performed using a potentiostat (Metrohm Autolab PGSTAT 302N). Electrochemical Impedance Spectroscopic (EIS) study was carried out in the frequency range 10^5 Hz to 0.1 Hz with an amplitude of 10 mV under no applied DC bias.

The corrosion efficiency of the coatings (in percentages) on mild steel surfaces were calculated by taking the corrosion rate of bare mild steel surface as a reference as 100%.

$$\text{The corrosion rate efficiency (percentages)} = \frac{\text{Corrosion rate of specific coating}}{\text{Corrosion rate of uncoated steel coating}} \quad (1)$$

Results and discussion

Natural muscovite sample and synthesised intermediate and final products

The formation of short chains of polymers or oligomers of PANI was confirmed in the experimental procedure by the appearance of thick and brown colour colloidal solution at the initial stage of polymerisation of the PANI. The continual process of polymerisation leads to long PANI polymer chains in which the colloidal turns blue-green at the final stage.[10] A schematic representation of the anticorrosive coatings is shown in Fig. 1 below.

The XRD spectrum of the raw mica material (Fig. 2d) reveals that it consists of peaks at 2θ values of 8.82°, 17.98°, 26.74°, 36.2°, 45.36°, and 54.92° are attributed to the corresponding basal planes of (002), (004), (006), (112), (0010), and (139) that can be assigned to muscovite (JCPDS card no. 01-089-5401). The muscovite consists of the chemical composition of $KAl_{2.20}(Si_3Al)_{0.975}O_{10}((OH)_{1.72}O_{0.28})$ with a monoclinic crystallographic structure. The intermediate product nano ground mica (nano-mica) shows similar XRD peak positions in the pattern with

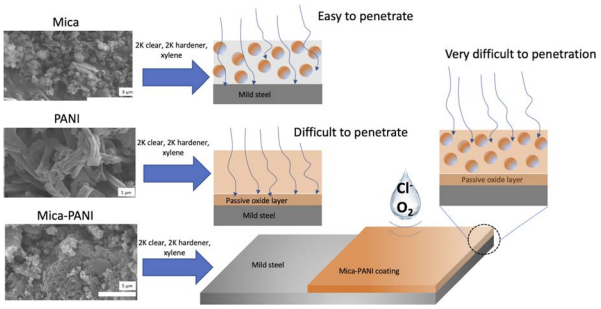

Fig. 1 Schematic representation of the anticorrosive coatings.

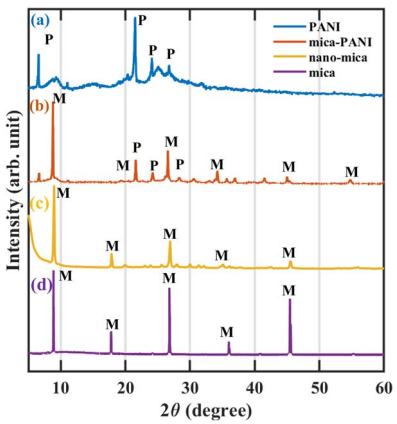

Fig. 2 XRD patterns of (a) PANI, (b) Mica–PANI composite, (c) nano-mica, and (d) mica.

the slight broadening of the peak that relates to the width of the peak due to increment in the high surface area and breakage along weaker cleavage planes (Fig. 2c). The pure PANI exhibit a sharp peak at the 2θ value of 21.13° and two other peaks around 24.29° and 26.99° with the corresponding planes (011), (020), and (200) respectively (Fig. 2a). The peaks at the 2θ values of 21.77° and 24.55° representing PANI are also observed in Fig. 2b, which indicates the PANI-coated nano-mica (mice-PANI). The XRD pattern of Mica–PANI consists of the peaks of both nano-mica and PANI, confirming the process of coating PANI on mica. The spectra reveal the certainty of the lattice structure of the formation of the nano-mica and polymer of PANI-coated nano-mica.

FE-SEM images of the raw, intermediate product materials "nano-mica and PANI" and the final product "Mica–PANI" are revealed in Fig. 3a–c, respectively, with different magnifications. Images of FE-SEM (Fig. 3a) describe the changes in the layered silicate structure of muscovite during the top-down approach of mechanical milling to produce nano-mica. It shows that muscovite's distinct layered silicate structure with sharp edges has changed to an agglomerated ball-like structure with an average particle diameter of 80 nm. Fig. 3b confirms the worm-like agglomerated heterogeneous polyaniline formation with the average particle length and width of 500 nm and 75 nm, respectively. A similar morphology of the PANI is observed as

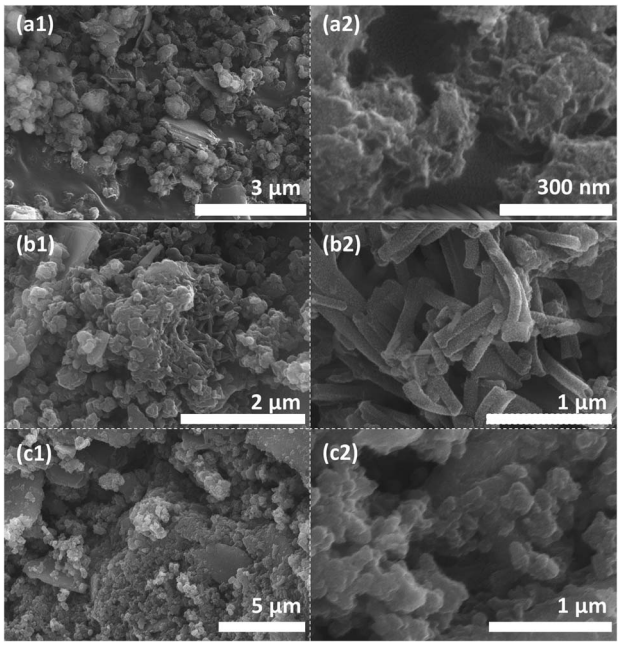

Fig. 3 The two different magnifications of the (a1) and (a2) nano-mica with low-focused and highly-focused images (b1) and (b2) PANI with low-focused and highly-focused images (c1) and (c2) Mica–PANI composite with low focused and highly-focused images.

the coating of the nanomica in the image Fig. 3c. It has an uneven surface with the blunted edges of muscovite. It is completely covered with PANI, which explains that nano-mica has offered the active sites to initiate the nucleation process of PANI during polymerisation.[9,10]

The chemical structure of the PANI, Mica–PANI, nano-mica and mica are illustrated in Fig. 4a–d, respectively. FT-IR spectrum confirms the presence of the synthesised intermediate nano-mica and product PANI-coated muscovite (Mica–PANI) by the appearance of the corresponding peaks. The characteristic band at 830–900 cm^{-1} in Fig. 4d is referred to the octahedral sheets occupied by a trivalent central atom O–H bending bands to the silicate sheets in the structure of muscovite.[19] The weak band at around 3624 cm^{-1} represents the stretching of the free hydroxyl group between tetrahedral and octahedral sheets in the structure of muscovite. The Al–OH group in the mica lattice does not show any peak due to no accessible reaction for steric hindrance. The bands in the range 600–750 cm^{-1} exhibit the bending vibrations of the Si–O bond.[20] The Al–O out-of-plane vibrations absorb at 810 cm^{-1}, and Al–O–Si in-plane vibrations absorb at 750 cm^{-1}. Liberational vibrations involving OH lie between 950–800 cm^{-1}.[19,21–23] The FT-IR spectra of nano-mica (Fig. 4c) show similar trend spectra like bulk mica with precise change. The peak around 3406 cm^{-1} displays a broad peak attributed to the hydroxyl (OH) group between tetrahedral and octahedral sheets. The difference between bulk and nano-mica is due to the rise in the surface area that leads to the effective vibration mode of the hydroxyl group.[24]

The characteristic bands (Fig. 4b) of Mica–PANI confirm the presence of PANI and Muscovite by the characteristic peaks of each compound. The presence of PANI is confirmed chemically in Fig. 4a. The characteristic bands at 2800 cm^{-1} to 3200 cm^{-1} are referred to as the stretching mode of N–H.[25] The bands at the ranges from 1697 cm^{-1} and 1470 cm^{-1} corresponded to C=N and C–C stretching modes for the quinoid and benzenoid rings.[9,10,26] The bands at about 1090 cm^{-1} have been referred to as the C–N stretching mode for the benzenoid ring. The band at 780 cm^{-1} is specified to an in-plane bending vibration of C–H (mode of N=Q=N, Q=N^+ H=B, and B–N^+ H–B; where Q is a quinonoid unit. B is a benzenoid unit) formed during protonation.[12,13] Similar bands detected at 3406 cm^{-1}, and 938 cm^{-1} represent the presence of characteristic muscovite in the final product Mica–PANI illustrated in Fig. 4b.

The thermal properties of the PANI, prepared composite Mica–PANI, nano-mica, and bulk mica, are interpreted using thermograms which are shown in Fig. 5a–d, respectively. The

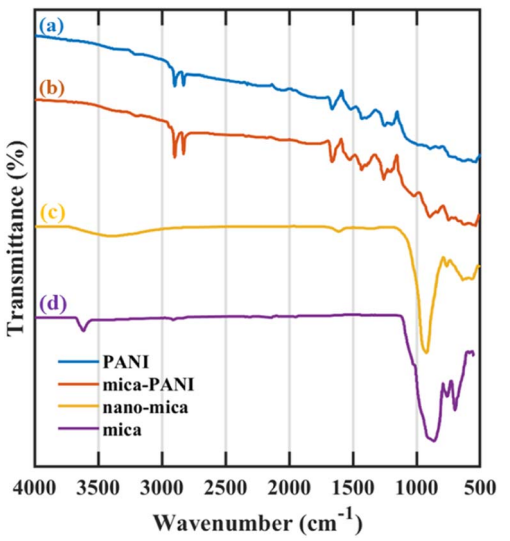

Fig. 4 FT-IR focused images in the ranges of wavenumber 4000–600 cm^{-1} of (a) PANI, (b) Mica–PANI composite, (c) nano-mica, and (d) mica.

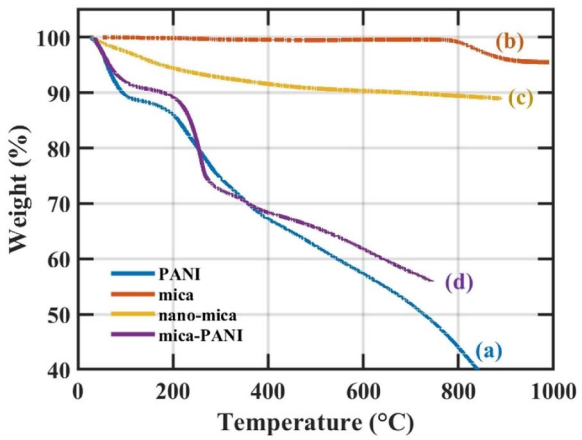

Fig. 5 TGA plots of (a) PANI, (b) Mica–PANI composite, (c) nano-mica, (d) mica.

TGA graphs of the nano-mica and Muscovite (Fig. 5c and d) interpret that muscovite exhibit higher thermal stability comparatively than the nano-mica due to lower surface area and lower concentration of free water molecule and a hydroxyl group. The mass-loss (0.37%) at the temperature range between 150 °C and 400 °C at the TGA curve of muscovite is due to adsorbed water that is different from simple moisture. In the case of nano-mica, the TGA curve shows two stages of weight loss at the temperature ranges between 100 –700 °C and 700–890 °C that show weight loss as 10.03% and 0.98%, respectively. The weight loss results from adsorbed water content and the removal of hydroxyl ions below the temperature of 890 °C. The total mass loss of muscovite and nano-mica is 4.7% and 11.01%, respectively.

The TGA curve of PANI (Fig. 5a) shows three stages of weight loss. The first weight loss of 11.37% at 130 °C is probably due to the evaporation of physisorbed water molecules. The second weight loss of 24.25% at the temperature of 460 °C can be attributed to the decomposition and evaporation of unreacted solvents. The third weight loss of 30.98% at the temperature of 907 °C is due to the degradation of the unsaturated group present in the polymer. The total weight loss of PANI is 66.6%. The TGA curve of composite Mica–PANI also exhibits a similar curve to PANI as it has the coating of the PANI on the surface of muscovite. However, the composite show comparatively higher thermal stability than the PANI as it consists of thermally stable nano-mica. The Mica–PANI composite exposes three stages of weight loss, as clearly indicated in Fig. 5b. The first weight loss of 8.97% in the composite's TGA curve can be associated with removing physisorbed water molecules *via* evaporation. The second weight loss at the temperature of 320 °C shows 19% due to the decomposition and evaporation of the unreacted solvents. 15% of weight loss in the third stage of the TGA curve can be related to the removal of hydroxyl ions of the muscovite nano-mica and the decomposition of the unsaturated group present in the polymer matrix. The TGA curve of the composite can be concluded that the composite is stable enough up to the temperature of 800 °C that the structure can be preserved due to the polymer coating.

Mechanism of composite of Mica–PANI formation

Muscovite composition, which is (K, Na)(Al, Mg, Fe)$_2$($Si_3Al_{2.90}$-$H_2KO_{12}Si_{3.10}$), has plenty of hydroxyl groups due to water adsorbed molecules on the surface of mica NPs. The electrochemical interaction between the carbonyl group of the stearic acid and the negatively surface-charged mica NPs forms the highly reactive COO^- group to the surface. The hydrogen bonding interaction between the surface hydroxyl groups, or the hydroxyl groups in ethanol, makes it possible to weaken the strong particle agglomeration of mica NPs and form a dispersion. Then, adding aniline to the mixed homogeneous suspension of HCl and mica NPs produces the adsorbed aniline on the surface of muscovite NPs due to the electrostatic interaction. When the initiative oxidant sodium persulfate is added to the solution, polymerisation is initiated just as at adsorbing sites producing a large number of PANI nuclei on the surface of the muscovite NPs by heterogeneous nucleation. The initial lower molecular weight positively charged PANI molecular chains would spontaneously be surrounded by free negative ions (Cl^-), forming an excellent protective layer to restrain the growth of PANI. The excess ionic liquids and ethanol can be washed out at the end of the polymerisation process.[12,27]

Anticorrosive property of prepared product Mica–PANI nanocomposites

Dynamical aspect of anticorrosive performance. Fig. 6a1 and a2 show Tafel plots for coatings with different weight percentages of Mica–PANI composites after reaching the initial equilibrium and after continuing to be in the corrosive conditions for 24 h respectively. According to Fig. 6a1, E_{corr} are most negative for bare mild steel at −0.8088 V and for the blank at −0.84339 V. For the 5% composite, E_{corr} is −0.68822 V. E_{corr} values of the 10% (−0.70924 V) and 16% (−0.66647 V) composites are not significantly different from that of 5% composite. J_{corr} is the lowest for the 5% composite material at 2.23×10^{-6} A cm^{-2} which is an order of magnitude lower than that of bare mild steel at 8.36×10^{-5} A cm^{-2}. According to E_{corr} and J_{corr}, the 5%, 10%, and 16% composite materials have significant and comparable anticorrosion activity compared to bare mild steel and the blank samples. Hence, the composite samples resulted the lowest corrosion rates of 2.7%, 3.9%, 3.1% are for 5%, 10%, and 16% composites respectively compared to the bare mild steel (100%) and the blank (86.7%) corrosion rates.

As shown in Fig. 6a2, even after 24 h, the composites showed better anticorrosion activity with less negative E_{corr} and smaller J_{corr} compared to that of bare steel and blank samples and hence lower corrosion rates. This 24 h result also indicates the appreciable composite coating stability. The weight percentage increase of Mica–PANI composites has not significantly improved the anticorrosion performance of the coating. This could be due to several reasons. At higher weight percentages it is possible that composite material aggregates[28] and the film integrity,[29] homogeneity,[30] diffusion properties,[31] and the

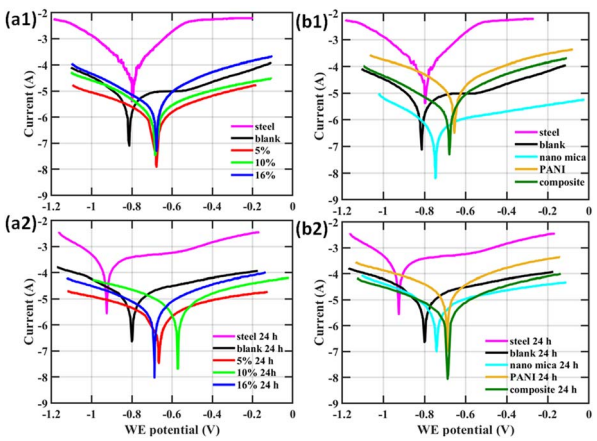

Fig. 6 Tafel plots of composition weight percentage (a1) initial (a2) 24 h and individual components at (b1) initial and (b2) 24 h after dipping the coating inside the 0.1 M, 30 mL NaCl solution.

Table 1 The composition of each prepared coating and the electrochemical parameters of the initial coatings and coatings dipping into the 0.1 M NaCl solution for 24 hours

	Content				Electrochemical corrosion studies				
Coating	Compound	2K clear (g)	2K hardener (g)	Xylene (g)	$E_{corr}\|E_{corr}$ 24 h (V)	$J_{corr}\|J_{corr}$ 24 h (A cm^{-2})	$R_p\|R_p$ 24 h (Ω)	$R_M\|R_M$ 24 h (mm per year)	$R_M\|R_M$ 24 h (%)
a	5% compo	2.5	0.625	3.3	−0.68822	2.23×10^{-6}	51 620	0.025958	2.7
					−0.66259	7.27×10^{-6}	29 380	0.08444	0.23
b	10% compo	2.5	0.625	3.3	−0.70924	2.66×10^{-6}	29 403	0.030895	3.9
					−0.57674	1.07×10^{-5}	11 158	0.12472	0.3
c	16% compo	2.5	0.625	3.3	−0.67273	2.57×10^{-6}	13 568	0.029855	3.1
					−0.69614	7.16×10^{-6}	12 534	0.08315	0.22
d	5% PANI	2.5	0.625	3.3	−0.66647	2.67×10^{-5}	3108.1	0.30973	31.9
					−0.69416	4.44×10^{-5}	2525.6	0.51567	1.4
e	5% mica NPs	2.5	0.625	3.3	−0.78363	3.54×10^{-6}	85 803	0.041167	4.2
					−0.76444	1.63×10^{-5}	9953.1	0.18946	0.5
f	Blank	2.5	0.625	3.3	−0.84339	7.25×10^{-5}	9355.2	0.84257	86.7
	—				−0.80752	1.28×10^{-4}	4345	1.4908	3.96
g	Commercial	—	—	—	−0.66857	5.76×10^{-6}	13 800	0.06688	6.9
					−0.72038	3.02×10^{-5}	37 503	0.35107	0.9
h	Uncoated	—	—	—	−0.8088	8.36×10^{-5}	404.72	0.97151	100
	mild steel				−0.93131	0.0032355	192.26	37.596	100

electrochemical performance[32] are altered. Moreover, 5% composite showed the highest R_p at 51 620 Ω compared to all other samples indicating the greater resistance to corrosion (Table 1).

Fig. 6b1 and b2 show Tafel plots for coatings with individual components of the composite, mica and PANI, after reaching the initial equilibrium and after continuing to be in the corrosive conditions for 24 h respectively. According to Fig. 6b1, E_{corr} are most negative for the bare mild steel at −0.8088 V and the blank at −0.84339 V. The lowest E_{corr} was obtained for PANI is −0.66647 V, which is comparable for that of the composite at −0.67273 V indicating the corrosion resistant nature. Similarly, J_{corr} are highest for the bare mild steel at 8.36×10^{-5} A cm^{-2} and the blank at 7.25×10^{-5} A cm^{-2}. J_{corr} are the lowest for composite material at 2.57×10^{-6} A cm^{-2} and then for mica at 3.54×10^{-6} A cm^{-2} which indicated the anticorrosion behaviour. Hence the composite has the lowest corrosion rate compared to that of bare mild steel, blank, and the individual components, mica (4.2%) and PANI (31.9%). A similar trend could be observed in Fig. 6b2 after 24 h as well. The variation of J_{corr} suggests that incorporation of mica NPs into the composite has enhanced the anticorrosive performance of coating as it acts as a barrier for the penetration of atmospheric oxygen and forming a passive layer on steel surface. In addition, mica has the highest R_p among all the samples, further confirming its great barrier effect for corrosion. The variation of E_{corr} shows that incorporation of PANI into the composite has enhanced the anticorrosive performance of coating *via* its electrochemical processes. This confirms that the composite of Mica–PANI significantly improved the anticorrosion performance of the coating compared to individual components due to combined barrier effect and electrochemical process of mica and PANI.

The Tafel plots in Fig. 7 show the initial and after 24 h comparison of the composite Mica–PANI with the commercially available anticorrosive paint. According to Fig. 7a, initially both the composite and the commercially available anticorrosion paint performs in a similar manner comparing E_{corr} and R_P. J_{corr} is better for the composite and hence smaller R_m and corrosion efficiency compared to the commercial paint. Interestingly, after 24 h, the composite had better values for E_{corr}, J_{corr}, R_P, R_m, and corrosion efficiency indicating a better anticorrosion activity. This confirms that the anticorrosion activity and the coating stability is superior in the composite.

Electrochemical impedance data. To compare the coating performance, electrochemical impedance spectroscopy was

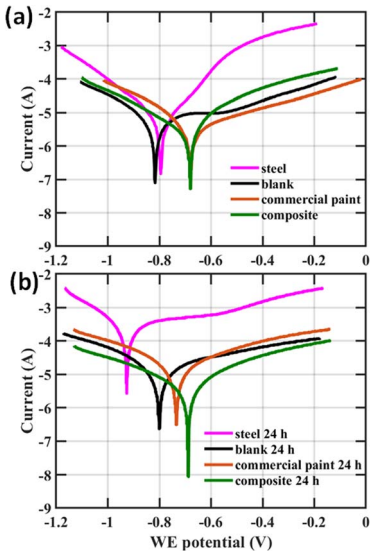

Fig. 7 Tafel plots for comparison of the Mica–PANI composite and commercial paint (a) initial equilibrium (b) 24 h after dipping the coating inside the 0.1 M, 30 mL NaCl solution.

done on the bare mild steel sample and the 5% composite sample. The equivalent circuits were fitted on electrochemical impedance data to understand the mechanism. Fig. 8a and b show the equivalent circuits for the bare mild steel and the 5% composite electrodes respectively where R_s is the solution resistance, R_{cp}, Q_{cp}, W, are the resistance of the corrosion product (oxide) layer, the capacitance of the corrosion product layer and the diffusion of materials respectively. C_c and R_c are the coating capacitance and the coating resistance respectively, where R_{ct} and Q_{dl} are the charge transfer resistance at the electrode interface and the electrochemical double layer capacitance respectively. Bare mild steel equivalent circuit shows evidence of high degree of corrosion susceptibility by having a low R_{ct} of 84.9 Ω and formation of a strong passivation oxide layer by having a high R_{cp} of 2290 Ω. The equivalent circuit for 5% composite sample shows the higher resistance of 554 Ω of R_c indicating the good coating performance and much lower R_{cp} of 401 Ω compared to bare mild steel sample indicating the mild formation of corrosion product layer. Most importantly, for the composite R_{ct} is significantly high as 1.05 KΩ compared to that of bare mild steel indicating the corrosion resistant behaviour at the metal interface. In addition, the exponent (N) of the Q_{dl} of the composite sample gives a much lower value of 0.308 compared to that of bare at 0.983 confirming the resistive nature at the metal interface when the coating is present. Therefore, impedance results confirm that the coating has excellent anticorrosion properties (Fig. 9).

Morphological aspect of anticorrosive performance. The images of the coated mild steel with the coatings of blank paint and composite paint which were dipped for 24 h inside the 0.1 M, 30 mL NaCl solution, are demonstrated in Fig. 10. The images clearly indicate that high corrosion protection is observed in composite and blank respectively.

Visual observations on the comparison of corrosion efficiency of coated mild steel with coatings blank paint and composite Mica–PANI paint against the bare mild steel and, which were dipped for 120 h into the solution of 0.1 M, 30 mL of NaCl solution were depicted in Fig. 11 below. The high corrosion protection is observed for the composite than that the blank paint and bare mild steel even after 120 h.

Fig. 12 below represents the graphical representation of percentage of corrosion rate efficiency R_M% for different paint coatings w.r.t. bare mild steel (100%). The synthesised Mica–PANI nanocomposite material exhibits the highest corrosion

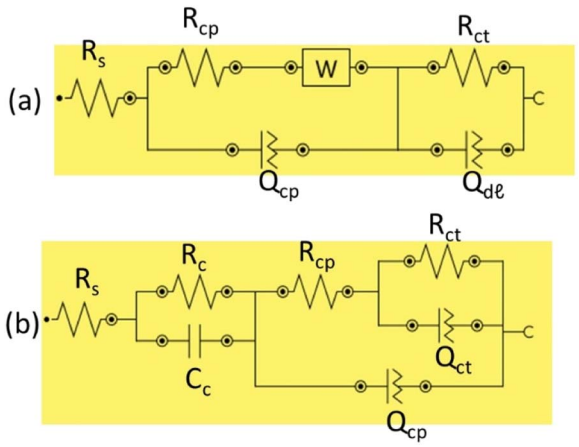

Fig. 8 Equivalent circuit used to obtain electrochemical impedance data.

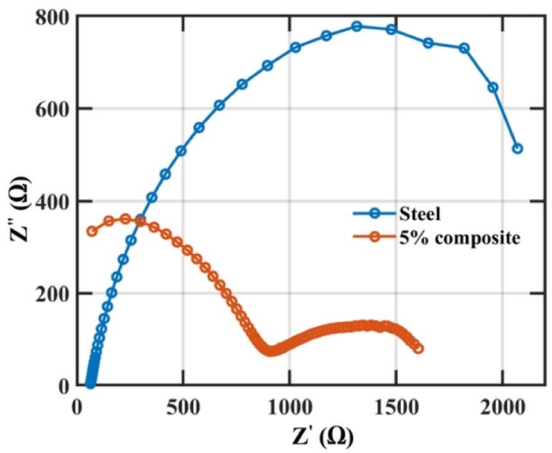

Fig. 9 Nyquist plot for electrochemical impedance data.

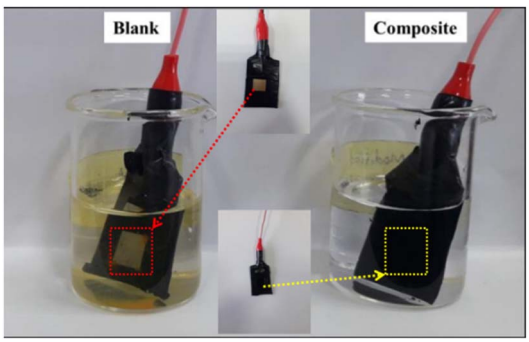

Fig. 10 Images of the comparison of the efficiency of the anticorrosive property of coating of blank and composite Mica–PANI paint after 24 h of dipping the coated mild steel inside 0.1 M, 30 mL of NaCl solution.

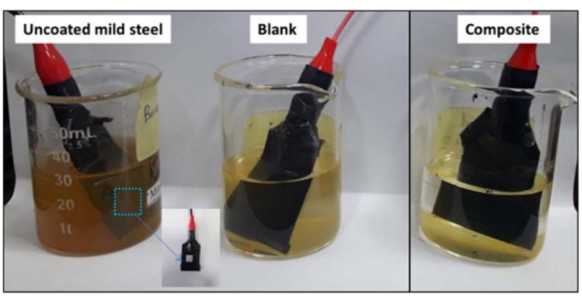

Fig. 11 Images of the comparison of the efficiency of the anticorrosive property of coating of blank, commercial paint, composite Mica–PANI with mild uncoated steel after 120 h of dipping the coated mild steel inside 0.1 M, 30 mL of NaCl solution.

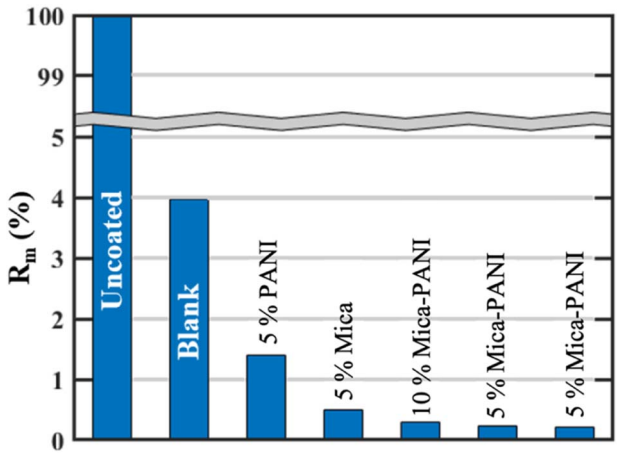

Fig. 12 Graphical representation of percentage of corrosion rate RM% for bare mild steel, blank coating, (16%) PANI coating, (16%) mica coating and composite paint coatings.

resistance of around 84 μm per year ($R_M \sim 0.23\%$) compared to blank sample of alkyd resin (1490 μm per year, 3.96%), existing commercial paint (351 μm per year, 0.9%), and other individual components such as PANI coatings (~516 μm per year, 1.4%) on mild steel surfaces. The results clarify that Mica–PANI nanocomposite is a challenging material for high-tech applications for surface coating.

Conclusions

Mica–PANI nanocomposite material was fabricated using natural muscovite and showed high potential as an anticorrosive coating on mild steel surfaces. The anticorrosive property study confirmed that the high anticorrosion protection of the product is mainly due to the electrochemical process and barrier effect through inhibition of corrosive agents like atmospheric O_2 and acidic environment. The muscovite mica in the composite product is attributed to high corrosion resistance due to its attractive properties, including high electrical and thermal insulation and chemically inertness. The synthesised eco-inspired Mica–PANI nanocomposite material exhibits the highest corrosion resistance of around 84 μm per year compared to blank sample of alkyd resin (1490 μm per year), existing commercial paint (351 μm per year), and other individual components such as PANI coatings (~516 μm per year) coated on mild steel surfaces. The results clarify that Mica–PANI nanocomposite is a challenging material for high-tech applications for surface coating. The study generally reveals prosperous novel techniques for fabricating Mica–PANI nanocomposite utilising naturally available muscovite mica and PANI. Furthermore, it indicates the capability of Mica–PANI nanocomposite as a highly anticorrosive and low-cost surface coating material for mild steel surfaces.

Author contributions

Anoja Senthilnathan: investigation, formal analysis, writing-original draft; D. M. S. N. Dissanayake: investigation, data curation; N. P. W. Rathuwadu: methodology, formal analysis, writing-review and editing, supervision; H. C. S. Perera: writing-review and editing, funding acquisition, project administration, validation; K. E. D. Y. T. Dayananda: writing-review and editing; K. R. Koswattage: supervision, resources, writing-review and editing; Rajesh Mahadeva: writing-review and editing, software, visualization; Arnab Ganguly: writing-review and editing, software, visualization; G. Das: writing-review and editing, resources, funding acquisition; M. M. M. G. P. G. Mantilaka: conceptualization, supervision, resources, writing-review and editing.

Conflicts of interest

There are no conflicts to declare.

Acknowledgements

M. M. M. G. P. G. M. and K. R. K. acknowledges the Science and Technology Human Resource Development Project, Ministry of Higher Education, Sri Lanka, funded by the Asian Development Bank (Grant no. CRG-R2-SB-1) and the National Research Council, Sri Lanka (Grant no. 19-064). G. D., H. C. S. P. and A. G. acknowledge the support of the Khalifa University internal funding FSU-2020-08 (8474000233) and CIRA-2021-071 (8474000416).

References

1 B. Kulyk, M. A. Freitas, N. F. Santos, F. Mohseni, A. F. Carvalho, K. Yasakau, A. J. S. Fernandes, A. Bernardes, B. Figueiredo, R. Silva, J. Tedim and F. M. Costa, *Crit. Rev. Solid State Mater. Sci.*, 2022, **47**, 309–355.
2 A. S. H. Makhlouf, *Handb. Smart Coatings Mater. Prot.*, 2014, pp. 121–131.
3 F. Olivieri, R. Castaldo, M. Cocca, G. Gentile and M. Lavorgna, *Nanoscale*, 2021, **13**, 9091–9111.
4 L. Liu, K. Shi, Y. Lu and C. Yu, *Micro Nano Lett.*, 2020, **15**, 728–731.
5 M. Faccini, L. Bautista, L. Soldi, A. M. Escobar, M. Altavilla, M. Calvet, A. Domènech and E. Domínguez, *Appl. Sci.*, 2021, **11**(8), 3446.
6 L. Nurdiwijayanto, H. Nishijima, Y. Miyake, N. Sakai, M. Osada, T. Sasaki and T. Taniguchi, *Nano Lett.*, 2021, **21**, 7044–7049.
7 D. Sazou and P. P. Deshpande, *Chem. Pap.*, 2017, **71**, 459–487.
8 Z. Tian, H. Yu, L. Wang, M. Saleem, F. Ren, P. Ren, Y. Chen, R. Sun, Y. Sun and L. Huang, *RSC Adv.*, 2014, **4**, 28195–28208.
9 K. G. C. Senarathna, M. M. M. G. P. G. Mantilaka, T. A. N. Peiris, H. M. T. G. A. Pitawala, D. G. G. P. Karunaratne and R. M. G. Rajapakse, *Electrochim. Acta*, 2014, **117**, 460–469.
10 R. M. N. M. Rathnayake, M. M. M. G. P. G. Mantilaka, M. Hara, H. H. Huang, H. W. M. A. C. Wijayasinghe,

M. Yoshimura and H. M. T. G. A. Pitawala, *Appl. Surf. Sci.*, 2017, **410**, 445–453.
11 E. Armelin, R. Pla, F. Liesa, X. Ramis, J. I. Iribarren and C. Alemán, *Corros. Sci.*, 2008, **50**, 721–728.
12 Y. Guo, D. He, S. Xia, X. Xie, X. Gao and Q. Zhang, *J. Nanomater.*, 2012, **2012**, 202794.
13 E. T. Kang, K. G. Neoh and K. L. Tan, *Prog. Polym. Sci.*, 1998, **23**, 277–324.
14 S. Chen, F. Chen, Y. Di, S. Han and X. Zhu, *Micro Nano Lett.*, 2020, **15**, 509–513.
15 A. Kalendová, *Pigm. Resin Technol.*, 2002, **31**, 216–225.
16 P. Kalenda, A. Kalendová, V. A. Štengl, P. Antoš, J. Šubrt, Z. Kváča and S. Bakardjieva, *Prog. Org. Coat.*, 2004, **49**, 137–145.
17 N. Maruthi, M. Faisal, N. Raghavendra, B. P. Prasanna, S. R. Manohara and M. Revanasiddappa, *Colloids Surf., A*, 2021, **621**, 126611.
18 D. K. Gupta, S. Neupane, S. Singh, N. Karki and A. P. Yadav, *Prog. Org. Coat.*, 2021, **152**, 106127.
19 W. Vedder and R. S. McDonald, *J. Chem. Phys.*, 1963, **38**, 1583–1590.
20 G. Mariotto, G. Das, A. Quaranta, G. Della Mea, F. Corni and R. Tonini, *J. Appl. Phys.*, 2005, **97**, 113502.
21 L. Cheng, D. Lin and K. Yang, *J. Membr. Sci.*, 2000, **172**, 157–166.
22 A. M. El-toni, S. Yin and T. Sato, *Appl. Surf. Sci.*, 2006, **252**, 5063–5070.
23 G. Das, G. Mariotto and A. Quaranta, *Mater. Sci. Semicond. Process.*, 2004, **7**, 295–300.
24 M. V Maslova, L. G. Gerasimova and W. Forsling, *Colloid J.*, 2004, **66**, 322–328.
25 N. Daldosso, G. Das, S. Larcheri, G. Mariotto, G. Dalba, L. Pavesi, A. Irrera, F. Priolo, F. Iacona and F. Rocca, *J. Appl. Phys.*, 2007, **101**, 113510.
26 Z. A. Boeva and V. G. Sergeyev, *Polym. Sci., Ser. C*, 2014, **56**, 144–153.
27 B. A. Bhanvase and S. H. Sonawane, *Chem. Eng. J.*, 2010, **156**, 177–183.
28 Y. Ge, X. Guo, D. Zhou and J. Liu, *Nanoscale*, 2022, **14**, 12358–12376.
29 W. Taleb, F. Pessu, C. Wang, T. Charpentier, R. Barker and A. Neville, *npj Mater. Degrad.*, 2017, **1**, 13.
30 S. Pourhashem, A. Rashidi, M. R. Vaezi and M. R. Bagherzadeh, *Surf. Coat. Technol.*, 2017, **317**, 1–9.
31 S. Pourhashem, M. R. Vaezi, A. Rashidi and M. R. Bagherzadeh, *Corros. Sci.*, 2017, **115**, 78–92.
32 Y. Zhao, S. Tian, D. Lin, Z. Zhang and G. Li, *Mater. Des.*, 2022, **216**, 110589.